Influence of the torsional potential on the glass transition temperature and the structure of amorphous polyethylene

Manel Canales*

Departament de Física i Enginyeria Nuclear, Universitat Politècnica de Catalunya, Campus Nord-Mòdul B4, c/Jordi Girona 1-3, 08034 Barcelona, Spain

(Received 18 December 2008; revised manuscript received 4 March 2009; published 28 May 2009)

The effect of the torsional potential on several thermodynamic and structural properties of a system of polyethylene chains has been analyzed. To this end, molecular dynamics simulations of a coarse-grained model, whose sites interact through a force field with bending, torsional, and nonbonded terms, have been considered. The torsional potential has three stable configurations: *gauche-*, *trans*, and *gauche+*. It has been modeled using a simple functional form with only two parameters: the *trans-gauche* and the *gauche-gauche* energy barriers. In order to analyze the influence of these parameters on the properties considered in this work, five models with different values of the torsional barriers have been considered. We have observed that the glass transition temperature, the intrachain radial distribution function, the radius of gyration, and the end to end distribution functions are very sensitive to the changes in the trans-gauche torsional barrier. Moreover, at low temperatures, the interchain radial distribution function, the orientational correlation function, and the volume distribution functions of the Voronoi polyhedra, that surround every site of the polymeric chains, also depend on the trans-gauche torsional barrier. On the contrary, the gauche-gauche energy barrier has a minor influence in the properties considered in this work.

DOI: 10.1103/PhysRevE.79.051802 PACS number(s): 64.70.pj, 34.20.Cf, 87.10.Tf, 82.35.Lr

I. INTRODUCTION

A great number of polymers are amorphous in nature. Their most important property is the glass transition temperature T_g which represents a signature of their internal structure [1]. According to the relation between the room temperature T_0 and T_g, amorphous polymers are [1]: elastomers and adhesives ($T_g < T_0$), plastics ($T_g > T_0$) and fibers, and house coatings and paints ($T_g \sim T_0$). During the last 50 years a great number of theories of the glass transition have been proposed [2–4], such as the free volume [5–8], the Simha-Somcynsky [9], the Gibbs-DiMarzio [10], the Adam-Gibbs [11], the inherent structures [12,13], the mode coupling [14,15], or the stochastic theory of volume relaxation [16,17]. In spite of these great efforts, the phenomenon of the glass transition is not completely well understood [18]. So, these theories explain some aspects, but it does not exist a unified description that puts all aspects into one coherent framework [19]. The study of the structure of polymers is also a very active research topic. So, the local structure can be analyzed through x-ray and neutron-diffraction experiments, being the total structure factor, with its intra- and intermolecular contributions, the most characteristic property [20–22]. During the last 30 years a great number of molecular dynamics (MD) and Monte Carlo (MC) computer simulations of polymeric systems have been performed in order to check theories, to interpret experimental data, or to get information about the microscopic behavior which cannot be measured experimentally [19,23–25].

Simulations and experiments have revealed that local relaxations in amorphous polymers are related to conformational dynamics, in particular with the torsional autocorrelation function. These and other characteristics of the local dynamics are ultimately linked with the glass transition [24,23]. These conclusions have encouraged some authors to study the influence of the torsional potential on T_g [26,27], the static structure factor, and some dynamical properties [28,29]. In a previous work we have studied the influence of the torsional potential on T_g for a coarse-grained model which mimics polyethylene [27]. Particularly, we performed MD simulations using several sets of torsional potentials with different *trans-gauche* (*t-g*) and *gauche-gauche* (*g-g*) barriers. In this preliminary study we determined T_g following the specific volume as a function of temperature, and we compared the results with some predictions of the free volume theory. In the present work we will analyze in more detail the influence of the torsional potential on T_g and in some structural properties, such as the orientational correlation function, the inter- and intraradial distribution functions and the distribution functions of the radius of gyration and the end to end distance.

The free volume approach of the glass transition is based on the idea that local rearrangements require some empty space or free volume. According to this theory, the glass transition occurs when the free available volume is smaller than a critical value [5–8,19]. Free volume can rigorously be defined for systems of hard spheres. However, several approaches have been used for more realistic systems [30], such as the one from Hiwatari, based on the cell model of a liquid [31], or the one proposed by Cohen and Grest [8] and Voloshin *et al.* [32], who have suggested that the volume of the Voronoi polyhedron which contains a particle may be considered as a measure of its free volume. Moreover, Voronoi analysis has been used to provide useful information of the local distribution of molecules for different systems, such as simple liquids [33,34], molecular liquids [35,36], and polymers [37–39]. In this work we also will study the influ-

*manel.canales@upc.edu

ence of the torsional potential on the distribution functions of the volume, area and shape of the Voronoi polyhedra associated to the sites of the polymeric chains.

The paper is organized as follows: the torsional potential and the simulation details are described in Sec. II. The influence of the torsional potential on T_g and the structural properties is studied, respectively, in the Secs. III and IV. The results of the Voronoi analysis are described in Sec. V. The main conclusions of the work are gathered in the last section.

II. SIMULATION DETAILS

Polyethylene has been studied at the coarse-grained level of description. To this end, systems with 5, 10, 20, 40, and 100 chains have been considered. In every case the chains have, respectively, 200, 100, 50, 25, and 10 sites, which play the role of the CH_2 and CH_3 groups of polyethylene. Sites interact through a potential which includes bending, torsional, and nonbonding terms. The bond length $l=1.54$ Å has been kept constant using the SHAKE algorithm [40]. The bending term has an harmonic dependence with parameters $k_\theta=57\,950$ K/rad^2 and $\theta_{eq}=112°$. Sites belonging to different chains and those pertaining to the same chain, but separated by four or more bonds, interact through a Lennard-Jones potential with parameters $\epsilon_{CH_3}=\epsilon_{CH_2}=49.3$ K and $\sigma_{CH_3}=\sigma_{CH_2}=3.94$ Å. In systems such as polyethylene the torsional potential shows three minima located at −120°, 0°, and 120°, which correspond, respectively, to the *gauche* [−](*g*−), *trans* (*t*), and *gauche* [+](*g*+) states. The torsional potential has been modeled by the equation,

$$V(\phi)=\frac{B_{gg}}{2}(1-\cos 3\phi), \quad -180° \le \phi \le -120°,$$

$$=\frac{B_{tg}}{2}(1-\cos 3\phi), \quad -120° < \phi < 120°,$$

$$=\frac{B_{gg}}{2}(1-\cos 3\phi), \quad +120° \le \phi \le 180°, \qquad (1)$$

where B_{tg} and B_{gg} are, respectively, the energy barriers between g ($g+$ or $g-$) and t states and between $g+$ and $g-$ states [27]. Because of the symmetry both $g+$ and $g-$ states are the same and will be called g. Five different torsional potentials, with the following energy barrier values, have been considered: T1($B_{tg}=B_{gg}=0$), T2($B_{tg}=6$ kJ/mol, $B_{gg}=0$), T3($B_{tg}=12.3$ kJ/mol, $B_{gg}=0$), T4($B_{tg}=12.3$ kJ/mol, $B_{gg}=20$ kJ/mol), and T5($B_{tg}=12.3$ kJ/mol, $B_{gg}=44.8$ kJ/mol). For sake of clarity in Fig. 1 we have only displayed the torsional models T4 and T5.

In order to calculate the volumetric glass transition temperature T_g, the following procedure has been applied: (1) a first configuration has been generated using the Susi method [41] at 1.35 cm^3/g and 500 K, which are the experimental values of polyethylene at 1 atm [42]. (2) Several millions of Monte Carlo motions, based on a reptation algorithm [43], have been applied to minimize the energy. (3) 4×10^5 MD time steps, using the Berendsen constant pressure (1 atm) and temperature (500 K) algorithm [44], have been performed in order to get the equilibrium configuration at the highest temperature. (5) Finally, a constant pressure (1 atm) cooling process with temperature steps of 5 K has been applied, in such a way that at every temperature the system has been equilibrated during 20 000 time steps and the volume has been computed during the last 5000.

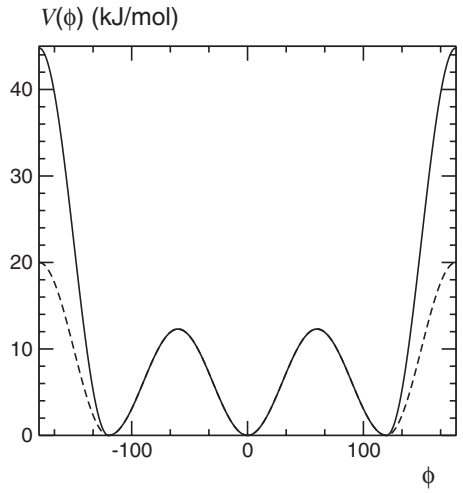

FIG. 1. Torsional potential of models T4 (dashed line) and T5 (continuous line).

The structural properties have been computed mainly for systems with 25 sites per chain N_{sc} because their radius of gyration and their end to end distance is less than the size of the cubic box, which is 30 Å. Previously, systems have been equilibrated at 50, 100, 200, and 300 K. To this end, the configurations obtained from the previous cooling process at those temperatures have been selected, and 4×10^5 MD time steps at constant pressure and temperature have been applied in order to compute the averaged volume value. Later, 4×10^5 MD time steps at constant volume, using this averaged volume value, have been performed in order to reach the equilibrated state. Finally, the structural properties have been calculated from the configurations generated during 10^6 MD time steps at constant volume. In all cases MD simulations have been performed using a cubic box with the usual periodic boundary conditions. Equations of motion have been solved using the leap frog Verlet algorithm [45] with a time step of 1 fs. The Lennard-Jones potential has been truncated at the cutoff distance of $2.5\sigma_{CH_2}$.

III. GLASS TRANSITION TEMPERATURE

Figure 2 shows the temperature dependence of the specific volume for systems with 10, 25, and 200 sites per chain (N_{sc}). For sake of clarity only the results obtained using the torsional potentials T1, T3, and T5 have been displayed. In all cases the two characteristic glass and rubber behaviors can be observed. Using a simple linear regression procedure, the data have been fitted to two straight lines, which intersect at $T=T_g$. The slopes α_G and α_R are, respectively, the expansion coefficients of the glassy and rubber states, and the intercepts v_{0G} and v_{0R} are the glass and rubber volumes ex-

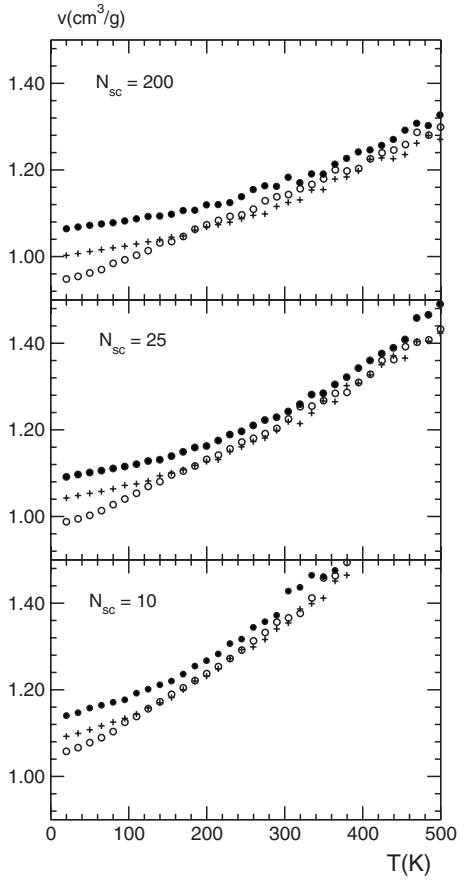

FIG. 2. Specific volume upon cooling at constant pressure (1 atm) for systems with N_{sc}=10, 25, and 200 sites per chain and torsional models T1 (open circles), T3 (crosses), and T5 (full circles).

trapolated at absolute zero [1]. These parameters, the differences between the expansion coefficients $\Delta\alpha=\alpha_R-\alpha_G$ and the volumes $\Delta v_0=v_{0G}-v_{0R}$, $T_g=\Delta v_0/\Delta\alpha$, $v_g=v(T=T_g)$, and the dimensionless quantities

$$K_1=\frac{\Delta\alpha T_g}{v_g} \quad \text{and} \quad K_2=\frac{\alpha_R T_g}{v_g} \tag{2}$$

have been gathered in Table I. Simha and Boyer [46] considered K_1 and Δv_0 as a measure of the free volume at T_g and 0 K. Moreover, they observed that for a wide variety of polymers K_1 and K_2 tend, respectively, to the values 0.113 and 0.164.

The results displayed in Fig. 2 and Table I show a clear decrease in α_G, α_R, $\Delta\alpha$, v_{0G}, v_{0R}, and v_g, and an increase in T_g (a decrease is observed for model T1) when N_{sc} rises. It is important to note that the systems simulated using the torsional models T3, T4, and T5, with the smallest number of sites per chain (N_{sc}=10), exhibit a lower T_g (147, 169, and 174 K, respectively) than those with greater N_{sc} values (for example, when N_{sc}=25, T_g=230, 216, and 223 K, respectively). Δv_0, $\Delta\alpha$, T_g, v_g, K_1, and K_2 always increase when B_{tg} rises regardless of N_{sc}. However, not noticeable differences are observed when B_{tg} is kept fixed and B_{gg} changes. Finally, it is also important to emphasize that K_1 and K_2 tend to the values reported by Simha and Boyer [46].

The K_1 and Δv_0 values gathered in Table I, calculated using the T1 and T2 models, are clearly smaller than those obtained from the other torsional potentials. Moreover, the Δv_0 and $\Delta\alpha$ computed from models T1 and T2 diminish when N_{sc} rises. In the particular case of the model T1, Δv_0 decreases more steeply than $\Delta\alpha$, and for this reason $T_g=\Delta v_0/\Delta\alpha$ also diminishes. Δv_0 decreases because the volume of the Voronoi polyhedron that surrounds an external site, which is a measure of its free volume, is more than 50% larger than the corresponding to an internal site (these details are explained in the Voronoi analysis section). As all the systems considered in this work have the same number of sites, if N_{sc} increases the number of chains (and the number of external sites) decreases and, as a result, the total free volume diminishes. On the contrary, simulations using models T3, T4, and T5 do not exhibit this behavior because their free volume is more influenced by the torsional forces, which increase the stiffness of the chains and therefore their free volume.

IV. STRUCTURAL PROPERTIES

The radial distribution function has two contributions: (1) the corresponding to sites that belong to the same chain, that is the intrachain radial distribution function $g_{intra}(r)$, and (2) the one from sites belonging to different chains, that is the interchain radial distribution function $g_{inter}(r)$ [24]. The $g_{intra}(r)$ at 300 K calculated for systems with torsional models T1, T3, and T5 and N_{sc}=25 are shown in Fig. 3. Differences in the torsional potentials give rise to noticeable variations in the local structure between 3 and 5 Å. So, the $g_{intra}(r)$ computed from the free torsional model (T1) shows a clear peak and two minor maxima located, respectively, at 3.9, 4.3, and 5.1 Å. If B_{tg} increases (and B_{gg}=0) the height of all maxima rises. Finally, if B_{gg} increases (and B_{tg} is kept fixed) a new maximum appears at 3.1 Å and the peak located at 4.3 Å shifts to slightly larger r values.

The $g_{inter}(r)$ calculated using the three torsional models at 50, 100, and 200 K are plotted in Fig. 4. It is important to note that the presence of some shoulders, rather than well defined peaks, in the second neighbor positions of the $g_{inter}(r)$ at 50 and 100 K is an indication that a crystallization process has probably been appeared at these temperatures [47]. Precisely, the differences between the results obtained using the three torsional potentials are only noticeable at 50 K. So, results using the free torsional model (T1) show two clear peaks located at 4.1 and 5.2 Å, being the first one the most important. If B_{tg} increases the first maximum decreases and the second becomes the most noticeable. Moreover, in this case the minimum and the maximum located around 7 and 9 Å shift to larger distances and become, respectively, one less depth and the other less heightened. On the contrary, if B_{tg} is kept fixed and B_{gg} increases the peak located at 4.1 Å diminishes and becomes a shoulder. Finally, it is important to note that our results at 200 and 300 K (not shown) are in a qualitative good agreement with those obtained by Tsige *et al.* for alkane chains at 430 K using a united atom model [25].

TABLE I. Expansion coefficients of the glassy α_G and rubber α_R states and their difference $\Delta\alpha$, glass v_{0G} and rubber v_{0R} volumes extrapolated at absolute zero and their difference Δv_0, glass transition temperature T_g, specific volume at the glass transition temperature v_g and the Simha and Boyer dimensionless parameters K_1 and K_2 for different models and number of sites per chain N_{sc}. α_G, α_R and $\Delta\alpha$ are expressed in $[10^{-4}\ \mathrm{cm}^3/(\mathrm{g\ K})]$, the volumes v_{0G}, v_{0R}, Δv_0, and v_g in cm^3/g, and T_g in K

N_{sc}	Model	α_G	α_R	$\Delta\alpha$	v_{0G}	v_{0R}	Δv_0	T_g	v_g	K_1	K_2
10	T1	6.86	11.41	4.55	1.043	1.013	0.030	66	1.089	0.028	0.069
25	T1	5.43	8.97	3.54	0.976	0.954	0.022	63	1.011	0.022	0.056
50	T1	5.17	7.95	2.78	0.955	0.937	0.018	64	0.988	0.018	0.052
100	T1	4.67	7.42	2.75	0.946	0.930	0.016	58	0.973	0.016	0.044
200	T1	4.77	7.24	2.47	0.938	0.925	0.013	54	0.964	0.014	0.041
10	T2	5.44	12.62	7.18	1.073	0.974	0.099	138	1.148	0.086	0.152
25	T2	3.66	8.97	5.31	1.010	0.936	0.074	140	1.062	0.070	0.118
50	T2	3.04	8.10	5.06	0.994	0.919	0.075	149	1.039	0.072	0.116
100	T2	2.67	7.44	4.77	0.984	0.917	0.067	141	1.022	0.066	0.103
200	T2	2.85	7.18	4.33	0.976	0.911	0.065	150	1.018	0.064	0.106
10	T3	5.79	12.89	7.10	1.079	0.975	0.104	147	1.165	0.090	0.163
25	T3	4.63	10.22	5.59	1.029	0.901	0.128	230	1.135	0.113	0.207
50	T3	3.87	8.51	4.64	1.012	0.908	0.104	224	1.098	0.094	0.173
100	T3	3.26	8.31	5.05	1.004	0.889	0.115	229	1.079	0.107	0.176
200	T3	3.35	8.01	4.66	0.994	0.882	0.112	240	1.074	0.104	0.179
10	T4	5.43	13.75	8.32	1.129	0.988	0.141	169	1.220	0.116	0.190
25	T4	3.60	10.26	6.66	1.079	0.935	0.141	216	1.157	0.124	0.192
50	T4	2.82	8.59	5.77	1.064	0.936	0.128	222	1.127	0.114	0.169
100	T4	2.52	8.13	5.61	1.060	0.929	0.131	234	1.119	0.117	0.170
200	T4	2.42	7.75	5.33	1.055	0.927	0.128	240	1.113	0.115	0.167
10	T5	6.03	13.69	7.66	1.125	0.992	0.133	174	1.230	0.108	0.194
25	T5	3.88	10.15	6.27	1.081	0.941	0.140	223	1.168	0.120	0.194
50	T5	3.03	8.46	5.43	1.069	0.943	0.126	232	1.140	0.111	0.172
100	T5	2.76	7.99	5.23	1.057	0.934	0.123	236	1.122	0.110	0.168
200	T5	2.68	7.84	5.16	1.058	0.931	0.127	246	1.124	0.113	0.172

The orientational correlation function gives information about the tendency of adjacent chains to align parallel and perpendicular to each other [24]. To define it, consider $\mathbf{b}_1$ as the vector connecting two adjacent bonds of a chain and $\mathbf{b}_2$ the one for a different chain. If r is the distance between the origins of both vectors, the function is defined as the ensemble average [48],

$$S(r) = \frac{1}{2}\langle 3[\mathbf{u}_1 \cdot \mathbf{u}_2]^2 - 1\rangle, \tag{3}$$

$\mathbf{u}_1$ and $\mathbf{u}_2$ being the $\mathbf{b}_1$ and $\mathbf{b}_2$ unit vectors. When $S(r)$ is positive there is a tendency for a parallel alignment, attaining the maximal value of 1. Negative values indicate a perpendicular alignment, −0.5 being the minimum value. For a random orientation $S(r)$ tends to zero.

$S(r)$ times $g_b(r)$ calculated using the three torsional models at 100, 200, and 300 K have been plotted in Fig. 5. $g_b(r)$

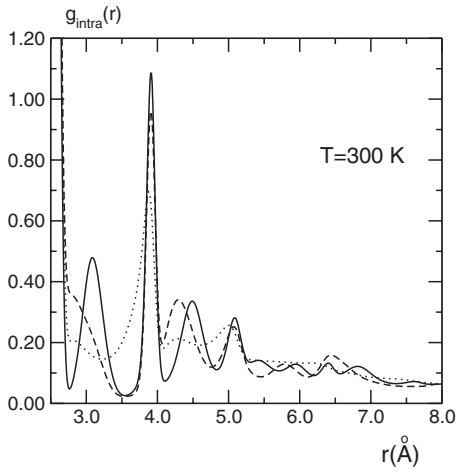

FIG. 3. Intrachain radial distribution function of systems with 25 sites per chain for models T1 (dotted line), T3 (dashed line), and T5 (continuous line).

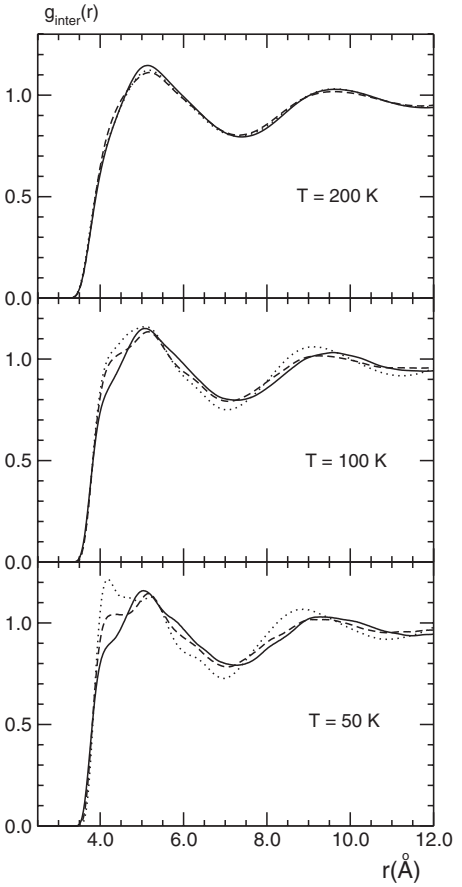

FIG. 4. Interchain radial distribution function for system with 25 sites per chain at several temperatures for models T1 (dotted line), T3 (dashed line), and T5 (continuous line).

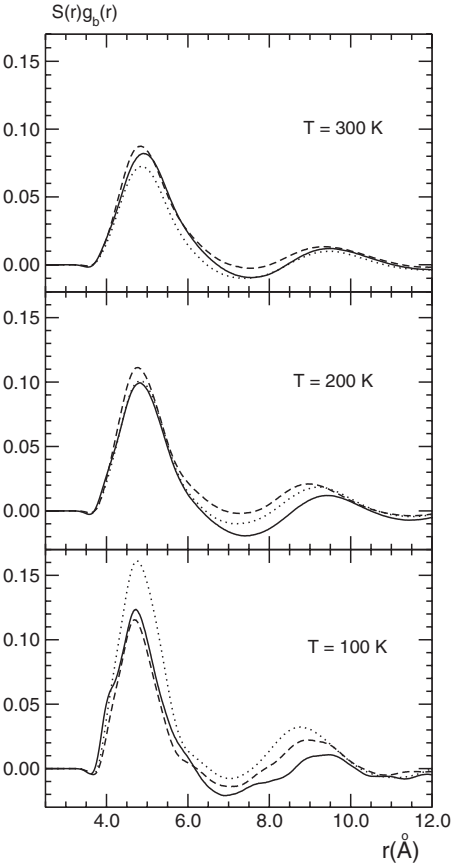

FIG. 5. Orientational correlation function times the interchain radial distribution function for system with 25 sites per chain at several temperatures for models T1 (dotted line), T3 (dashed line), and T5 (continuous line).

is the radial distribution function between the origins of the vectors $\mathbf{b}_1$ and $\mathbf{b}_2$, that at the same time is $g_{inter}(r)$. In all cases two clear peaks and two minima located, respectively, at 4.8, 9.5, 7.5, and 12 Å are observed, which correspond to the first and second coordination shells of the polymeric chains. The differences between the results obtained using the three models are particularly noticeable at 100 K. So, the $S(r)g_b(r)$ computed from the free torsional model (T1) is nearly positive for all distances. But if B_{tg} increases the second peak shifts to larger r values, the height of the maxima decreases and the depth of the first minimum increases, becoming more negative. Moreover, if B_{tg} is kept fixed and B_{gg} increases: (1) the second maximum also shifts to larger distances and its height diminishes and (2) the first minimum becomes more negative. So, simulations using the torsional models T3 and T5 show a clear tendency to have both the parallel and perpendicular alignment.

The radius of gyration R_g and the end to end distance R_{ee} gives a picture of the size of the chains. The probability distribution of the square of the radius of gyration R_g^2, calculated using models T1, T3, and T5 at 300 K, have been plotted in Fig. 6. The mean values ($\mu_{R_g^2}$ and $\mu_{R_{ee}^2}$) and their standard deviations ($\sigma_{R_g^2}$ and $\sigma_{R_{ee}^2}$), calculated for all torsional models at 300 K, have been gathered in Table II. It can be observed that $\mu_{R_g^2}$ and $\mu_{R_{ee}^2}$ increase when B_{tg} rises. So, the mean values obtained using the T3 torsional model are 8% and 13% larger than those calculated from the free torsional model. Moreover, our results also indicate that B_{gg} has not remarkable influence in the distribution functions and their mean values.

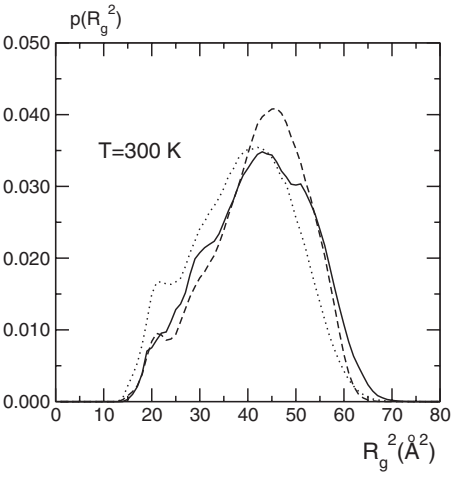

FIG. 6. Probability distribution function of the square of the radius of gyration calculated using models T1 (dotted line), T3 (dashed line), and T5 (continuous line).

TABLE II. Mean values $(\mu_{R_g^2}, \mu_{R_{ee}^2})$ and standard deviations $(\sigma_{R_g^2}, \sigma_{R_{ee}^2})$ of the square of the radius of gyration R_g and the end to end distance R_{ee} distribution functions at 300 K. All quantities are given in Å^2.

Model	$\mu_{R_g^2}$	$\sigma_{R_g^2}$	$\mu_{R_{ee}^2}$	$\sigma_{R_{ee}^2}$
T1	38.8	10.5	295	148
T2	39.5	10.5	302	153
T3	42.1	10.0	338	151
T4	42.9	10.5	340	154
T5	42.2	10.5	328	155

V. VORONOI ANALYSIS

The Voronoi polyhedron (VP) of a given site is the region of space containing all points closer to this site than to any other [49]. Several authors have proposed algorithms to make Voronoi tesselations [34,49–52]. In this work we use the simple method of Tokita *et al.* [39]. So, every VP is constructed applying the following procedure: (1) select a site that will be the center of the polyhedron. (2) Consider all the possible sites that are at a given distance of this center. (3) Construct a bisecting plane perpendicular to the line between the center and one of these sites. (4) Repeat the previous procedure for all the sites selected in step 2. (5) Consider a set of three of these planes and compute the intersection point. (6) Verify that this point is inside the polyhedron. If so, the point will be a vertex of the polyhedron. (7) Repeat the procedures 5 and 6 for all the possible triads of planes and determine all the vertex of the polyhedron. (8) Compute the faces and edges. (9) Check the Euler relation, which states,

$$v - e + f = 2, \tag{4}$$

v, e, and f being, respectively, the number of vertex, edges, and faces of every VP. From the vertex positions it is possible to compute the volume V, the surface of every face, the total surface S of the polyhedron and the asphericity or shape factor η, which is a dimensionless parameter defined as [38]

$$\eta = \frac{S^3}{36\pi V^2}. \tag{5}$$

By definition η is 1 for a sphere and takes larger values for nonspherical objects. So, for example, it equals 1.33, 1.35, and 1.91 for a truncated octahedron, a rhombic dodecahedron and a cube, respectively.

60 years ago Fox and Flory [5] observed that the glass transition temperature of polymers increases with the chain length. They explained this dependence assuming that the free volume around a chain end is larger than the corresponding to an internal site. Afterward, Rigby and Roe [37] and Tokita *et al.* [39] made simulations of polymeric systems, where they computed both the VP containing internal and end sites, and they verified that end sites occupy larger volumes than internal sites. In the present study we have also calculated the VP of both internal and end sites.

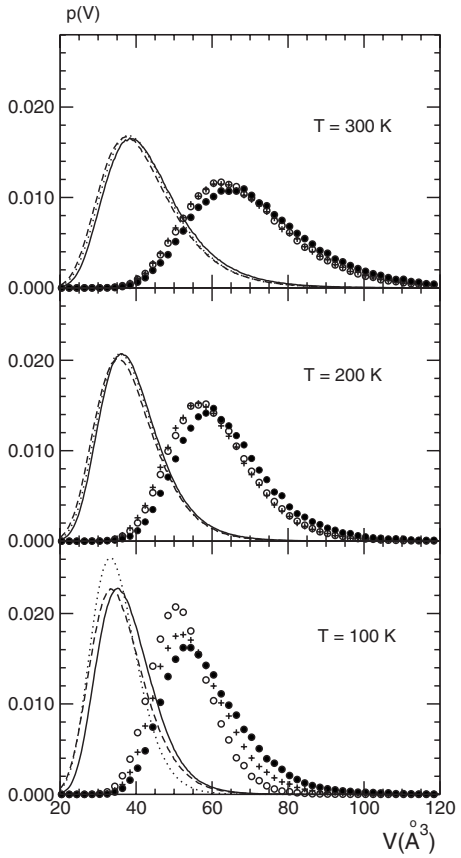

FIG. 7. Volume distribution functions of the Voronoi polyhedra that surround internal (lines) and end (symbols) sites at several temperatures obtained using the T1 (dotted line and open circles), T3 (dashed line and crosses), and T5 (continuous line and full circles) torsional models.

The volume distribution functions of the VP that surround internal $p(V_{int})$ and end $p(V_{end})$ sites at 100, 200, and 300 K, obtained using the T1, T3, and T5 torsional models, are plotted in Fig. 7. Moreover, the mean volume values $(\mu_{V_{int}}, \mu_{V_{end}})$ and their standard deviations $(\sigma_{V_{int}}, \sigma_{V_{end}})$ of internal and end sites, computed using the five torsional potentials at 50, 100, 200, and 300 K, are gathered in Table III. In all cases $\mu_{V_{int}} < \mu_{V_{end}}$ and $\sigma_{V_{int}} < \sigma_{V_{end}}$. This result can be explained taking into account that: (1) internal sites are bonded to two adjacents and end sites to only one, and (2) the distance between bonded sites is always smaller than the one between nonbonded sites. As can be observed in Table III and Fig. 7, the distribution functions are sensitive to the torsional potential barriers. So, above T_g (for example 300 K) $\mu_{V_{end}}$ and $\mu_{V_{int}}$ do not substantially change if B_{tg} increases and $B_{gg}=0$, but they slightly rise if B_{gg} increases and B_{tg} is kept fixed. However, at low temperatures (for example 100 K) $\mu_{V_{end}}$ and $\mu_{V_{int}}$ rise when both torsional barriers increase. This behavior is clearly related with the results of the three dilatometric curves shown in Fig. 2. In this case, at low temperatures, the specific volume increases when both B_{tg} and B_{gg} barriers rise. However, above T_g (for example 300 K) the specific volumes of the systems simulated using models T1 and T3 coincide, but they are slightly smaller than those of model T5.

TABLE III. Mean values ($\mu_{V_{int}}, \mu_{V_{end}}, \mu_{\eta_{int}}, \mu_{\eta_{end}}$) and standard deviations ($\sigma_{V_{int}}, \sigma_{V_{end}}, \sigma_{\eta_{int}}, \sigma_{\eta_{end}}$) of the volume ($V$) and asphericity ($\eta$) of the Voronoi polyhedra associated to internal and end sites for different models and temperatures. The ratio ($\mu_{V_{end}}/\mu_{V_{int}}$) of the volumes of the VP associated to end and internal sites is also included. $\mu_{V_{int}}$, $\mu_{V_{end}}$, $\sigma_{V_{int}}$, and $\sigma_{V_{end}}$ are expressed in Å^3 and temperatures in K.

Model	T	$\mu_{V_{int}}$	$\sigma_{V_{int}}$	$\mu_{V_{end}}$	$\sigma_{V_{end}}$	$\frac{\mu_{V_{end}}}{\mu_{V_{int}}}$	$\mu_{\eta_{int}}$	$\sigma_{\eta_{int}}$	$\mu_{\eta_{end}}$	$\sigma_{\eta_{end}}$
T1	50	33.0	5.5	48.3	6.8	1.46	2.26	0.67	1.73	0.43
T1	100	35.0	6.5	52.5	8.2	1.50	2.24	0.70	1.77	0.47
T1	200	38.9	8.6	60.7	11.5	1.56	2.20	0.75	1.75	0.51
T1	300	42.8	11.1	68.8	15.6	1.61	2.14	0.79	1.72	0.55
T2	50	34.7	6.5	50.8	7.1	1.46	2.25	0.70	1.81	0.46
T2	100	35.6	6.9	53.5	8.5	1.50	2.25	0.72	1.80	0.47
T2	200	38.5	8.7	60.3	11.5	1.56	2.24	0.75	1.75	0.50
T2	300	42.3	11.2	68.0	15.4	1.61	2.21	0.79	1.73	0.54
T3	50	35.5	7.5	53.3	9.2	1.50	2.29	0.73	1.80	0.49
T3	100	36.3	7.8	55.5	9.9	1.53	2.29	0.74	1.77	0.50
T3	200	38.6	8.8	60.0	11.5	1.55	2.27	0.76	1.75	0.49
T3	300	42.4	11.4	68.6	15.8	1.62	2.23	0.79	1.72	0.53
T4	50	37.2	7.6	58.3	9.8	1.57	2.36	0.73	1.75	0.47
T4	100	37.8	7.9	59.0	9.8	1.56	2.35	0.74	1.77	0.48
T4	200	39.8	8.9	62.9	12.4	1.58	2.33	0.76	1.80	0.52
T4	300	43.3	11.5	70.9	16.5	1.64	2.28	0.79	1.76	0.55
T5	50	37.4	7.4	57.9	11.3	1.55	2.32	0.74	1.84	0.53
T5	100	37.9	7.6	58.6	11.4	1.55	2.32	0.74	1.84	0.53
T5	200	39.6	8.9	63.8	12.8	1.61	2.36	0.76	1.80	0.53
T5	300	43.9	11.7	71.5	16.7	1.63	2.25	0.79	1.75	0.55

Rigby and Roe [37] observed that $\mu_{V_{int}}$ and $\mu_{V_{end}}$ shift to larger values and that $p(V_{int})$ and $p(V_{end})$ become broader ($\sigma_{V_{int}}$ and $\sigma_{V_{end}}$ increase) when the temperature rises. We have noticed the same behavior and, in addition, we have observed that this increase is not the same for the different torsional potentials. So, at 300 K the $\mu_{V_{end}}$ and $\mu_{V_{int}}$ calculated using the free torsional model are, respectively, 40% and 30% larger than those at 50 K. However, these values are reduced to 24% and 15% when the T5 potential has been considered. Moreover, the ratio between the mean volume values $\mu_{V_{end}}/\mu_{V_{int}}$ slightly increases when the temperature rises. These results can be easily explained taking into account that systems expand when temperature rises. Rigby and Roe [37] also noted that at high temperatures $p(V_{int})$ and $p(V_{end})$ are broad but become narrower as the temperature is lowered close to T_g. So, we have observed that at 300 K the standard deviations of the volume distribution functions calculated using the different torsional models are $\sigma_{V_{int}}=11.1-11.7$ Å^3 and $\sigma_{V_{end}}=15.6-16.7$ Å^3. As the glass transition temperature of the systems simulated using the models T3, T4, and T5 are between 216 and 230 K, the standard deviations at temperatures close to their T_g have been reduced, respectively, to 9 and 13 Å^3. Moreover, for the systems which have been simulated using models T1 and T2 the standard deviations have been reduced even more (7 and 9 Å^3) because in these cases T_g is smaller (63 and 140 K, respectively).

The asphericity distribution functions of the VP, that surround internal $p(\eta_{int})$ and end $p(\eta_{end})$ sites, and the mean values of the asphericity ($\mu_{\eta_{int}}, \mu_{\eta_{end}}$) and their standard deviations ($\sigma_{\eta_{int}}, \sigma_{\eta_{end}}$), computed using the different torsional models at several temperatures, are, respectively, shown in Fig. 8 and Table III. In all cases $\mu_{\eta_{int}} > \mu_{\eta_{end}} > 1$. This result indicates that the VP associated to the end sites tend to be more spherical than the ones of the internal sites. Moreover, the mean values are not substantially modified when the temperature and the different torsional potential barriers are changed. This result can be explained taking into account that these changes have similar effects in both the surface and the volume of the VP and, as a consequence, not in the shape of the polyhedra [see formula (5)].

The distribution functions of the number of faces and vertex of the VP, that surround internal $p(f_{int})$ and end $p(f_{end})$ sites, and the mean values of the number of faces and vertex corresponding to the internal ($\mu_{f_{int}}$ and $\mu_{v_{int}}$) and end ($\mu_{f_{end}}$

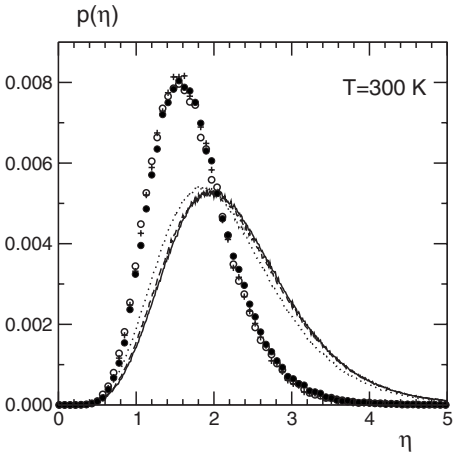

FIG. 8. Asphericity distribution functions of the Voronoi polyhedra that surround internal (lines) and end (symbols) sites obtained using the T1 (dotted line and open circles), T3 (dashed line and crosses), and T5 (continuous line and full circles) torsional models.

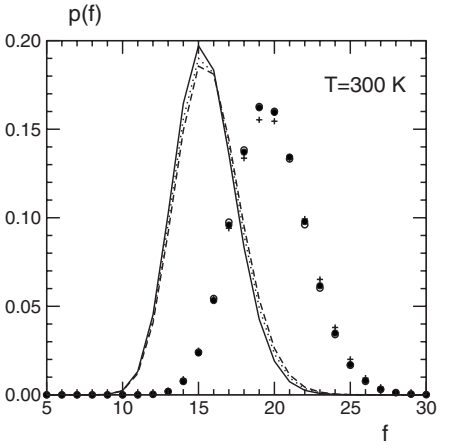

FIG. 9. Distribution functions of the number of faces of the Voronoi polyhedra that surround internal (lines) and end (symbols) sites obtained using the T1 (dotted line and open circles), T3 (dashed line and crosses), and T5 (continuous line and full circles) torsional models.

and $\mu_{v_{end}}$) sites and their standard deviations ($\sigma_{f_{int}}$, $\sigma_{v_{int}}$, $\sigma_{f_{end}}$, and $\sigma_{v_{end}}$), calculated from all the torsional potentials at several temperatures, are displayed, respectively, in Fig. 9 and Table IV. The number of faces and vertex of the VP associated to the internal sites are, respectively, 15.5 and 27, and 19.5 and 35 for the external sites. Moreover, the VP associated to the internal and end sites have, respectively, 5.2 and 5.4 vertex per face. These results do not substantially change with the height of the torsional potential barriers and the temperature.

TABLE IV. Mean values ($\mu_{f_{int}}, \mu_{f_{end}}, \mu_{v_{int}}, \mu_{v_{end}}$) and standard deviations ($\sigma_{f_{int}}, \sigma_{f_{end}}, \sigma_{v_{int}}, \sigma_{v_{end}}$) of the number of faces (f) and vertex (v) of the Voronoi polyhedra associated to internal and end sites for different models and temperatures. Temperatures are given in K.

Model	T	$\mu_{f_{int}}$	$\sigma_{f_{int}}$	$\mu_{f_{end}}$	$\sigma_{f_{end}}$	$\mu_{v_{int}}$	$\sigma_{v_{int}}$	$\mu_{v_{end}}$	$\sigma_{v_{end}}$
T1	50	15.5	1.7	18.5	1.9	27.0	3.4	33.0	3.9
T1	100	15.5	1.8	18.9	2.1	27.0	3.6	33.8	4.1
T1	200	15.6	2.0	19.4	2.3	27.2	3.9	34.7	4.5
T1	300	15.6	2.1	19.7	2.4	27.2	4.2	35.3	4.9
T2	50	15.7	1.8	18.9	1.9	27.4	3.6	33.8	3.8
T2	100	15.7	1.8	19.2	2.1	27.4	3.6	34.4	4.1
T2	200	15.7	2.0	19.4	2.3	27.3	3.9	34.9	4.6
T2	300	15.7	2.1	19.7	2.5	27.3	4.3	35.5	5.0
T3	50	15.7	1.9	19.0	2.0	27.4	3.7	34.0	4.0
T3	100	15.7	1.9	19.2	2.1	27.4	3.8	34.5	4.2
T3	200	15.7	2.0	19.5	2.3	27.4	4.0	34.9	4.6
T3	300	15.7	2.1	19.8	2.5	27.4	4.3	35.5	5.1
T4	50	15.4	1.8	19.1	2.0	26.9	3.6	34.2	4.0
T4	100	15.4	1.8	19.1	2.0	26.9	3.7	34.1	4.0
T4	200	15.5	1.9	19.5	2.3	27.0	3.8	34.9	4.5
T4	300	15.5	2.0	19.7	2.5	27.0	4.1	35.4	4.9
T5	50	15.4	1.8	19.2	2.4	26.9	3.6	34.5	4.8
T5	100	15.5	1.8	19.2	2.3	26.9	3.7	34.3	4.5
T5	200	15.5	1.9	19.4	2.2	26.9	3.8	34.9	4.5
T5	300	15.5	2.0	19.7	2.4	26.9	4.1	35.4	4.9

VI. CONCLUSIONS

Thermodynamic properties such as the glass transition temperature T_g and the specific volume at T_g increase when the *trans-gauche* torsional potential barrier B_{tg} rises. Moreover, the peaks of the intrachain radial distribution function $g_{intra}(r)$, and the mean values of the distribution functions of the square of the radius of gyration $\mu_{R_g^2}$ and the end to end distance $\mu_{R_{ee}^2}$, also rise when B_{tg} increases. It is also important to note that the K_1 and K_2 coefficients defined in formula (2) tend to the values reported by Simha and Boyer, and that systems with very short chains ($N_{sc}=10$) have a smaller T_g than those with larger N_{sc} values.

The remaining structural properties are only sensitive to B_{tg} at low temperatures. So, the interchain radial distribution function $g_{inter}(r)$ and the orientational correlation function $S(r)$ peaks are lower, appear at larger distances, and the values of the first minimum of $S(r)g_b(r)$ become more negative, when B_{tg} increases. The mean volume values of the distribution of the Voronoi polyhedra VP associated to the internal and end sites increase when B_{tg} and B_{gg} rise, being more noticeable for the end sites at low temperatures. Moreover, the VP have a tendency to keep their form (asphericity) and their number of faces and vertex when B_{tg} or the temperature increase. Finally, it should be noted that the *gauche-gauche* torsional barrier B_{gg} has a minor influence in all these properties.

ACKNOWLEDGMENTS

Financial support of DGICYT (Project No. FIS2006-12436-C02-01) and of Generalitat de Catalunya (Project No. 2005SGR00779) is acknowledged.

[1] L. H. Sperling, *Introduction to Physical Polymer Science* (Wiley, Hoboken, 2006).
[2] P. G. Debenedetti, *Metastable Liquids: Concepts and Principles* (Princeton University Press, Princeton, 1996).
[3] P. G. Debenedetti and F. H. Stillinger, Nature (London) **410**, 259 (2001).
[4] C. A. Angell, K. L. Ngai, G. B. McKenna, P. F. McMillan, and S. W. Martin, J. Appl. Phys. **88**, 3113 (2000).
[5] T. G. Fox and P. J. Flory, J. Appl. Phys. **21**, 581 (1950).
[6] M. H. Cohen and D. Turnbull, J. Chem. Phys. **31**, 1164 (1959).
[7] D. Turnbull and M. H. Cohen, J. Chem. Phys. **52**, 3038 (1970).
[8] M. H. Cohen and G. S. Grest, Phys. Rev. B **20**, 1077 (1979).
[9] R. Simha and T. Somcynsky, Macromolecules **2**, 342 (1969).
[10] J. H. Gibbs and E. A. DiMarzio, J. Chem. Phys. **28**, 373 (1958).
[11] G. Adam and J. H. Gibbs, J. Chem. Phys. **43**, 139 (1965).
[12] F. H. Stillinger and T. A. Weber, Phys. Rev. A **25**, 978 (1982).
[13] F. H. Stillinger and T. A. Weber, Phys. Rev. A **28**, 2408 (1983).
[14] W. Götze and L. Sjögren, Rep. Prog. Phys. **55**, 241 (1992).
[15] W. Götze, *Complex Dynamics of Glass-Forming Liquids* (Oxford University Press, New York, 2009).
[16] R. E. Robertson, R. Simha, and J. G. Curro, Macromolecules **17**, 911 (1984).
[17] R. E. Robertson, R. Simha, and J. G. Curro, Macromolecules **18**, 2239 (1985).
[18] P. W. Anderson, Science **267**, 1615 (1995).
[19] K. Binder, J. Baschnagel, and W. Paul, Prog. Polym. Sci. **28**, 115 (2003).
[20] R. J. Roe, *Methods of X-Ray and Neutron Scattering in Polymer Science* (Oxford University Press, New York, 2000).
[21] K. G. Honnell, J. D. McCoy, J. G. Curro, K. Schweizer, A. Narten, and A. Habenschuss, J. Chem. Phys. **94**, 4659 (1991).
[22] J. D. Londono, A. Habenschuss, J. G. Curro, and J. J. Rajasekaran, J. Polym. Sci., Part B: Polym. Phys. **34**, 3055 (1996).
[23] R. Boyd and G. D. Smith, *Polymer Dynamics and Relaxation* (Cambridge University Press, Cambridge, England, 2007).
[24] W. Paul and G. D. Smith, Rep. Prog. Phys. **67**, 1117 (2004).
[25] M. Tsige, J. G. Curro, G. S. Grest, and J. D. McCoy, Macromolecules **36**, 2158 (2003).
[26] R. H. Gee and R. H. Boyd, Comput. Theor. Polym. Sci. **8**, 93 (1998).
[27] M. Canales and G. Sesé, J. Mol. Liq. **136**, 206 (2007).
[28] S. Krushev and W. Paul, Phys. Rev. E **67**, 021806 (2003).
[29] W. Paul, Polymer **45**, 3901 (2004).
[30] F. W. Starr, S. Sastry, J. F. Douglas, and S. C. Glotzer, Phys. Rev. Lett. **89**, 125501 (2002).
[31] Y. Hiwatari, J. Chem. Phys. **76**, 5502 (1982).
[32] V. P. Voloshin, Y. I. Naberukhin, N. N. Medvedev, and M. S. Jhon, J. Chem. Phys. **102**, 4981 (1995).
[33] A. Rahman, J. Chem. Phys. **45**, 2585 (1966).
[34] J. C. Gil Montoro and J. L. F. Abascal, J. Phys. Chem. **97**, 4211 (1993).
[35] P. Jedlovszky, J. Chem. Phys. **111**, 5975 (1999).
[36] G. Ruocco, M. Sampoli, and R. Vallauri, J. Chem. Phys. **96**, 6167 (1992).
[37] D. Rigby and R. J. Roe, Macromolecules **23**, 5312 (1990).
[38] M. Sega, P. Jedlovszky, N. N. Medvedev, and R. Vallauri, J. Chem. Phys. **121**, 2422 (2004).
[39] N. Tokita, M. Hirabayashi, C. Azuma, and T. Dotera, J. Chem. Phys. **120**, 496 (2004).
[40] J. P. Ryckaert, G. Cicotti, and H. J. C. Berendsen, J. Comput. Phys. **23**, 327 (1977).
[41] D. Curcó and C. Alemán, J. Chem. Phys. **119**, 2915 (2003).
[42] O. Olabisi and R. Simha, Macromolecules **8**, 206 (1975).
[43] N. G. Almarza, E. Enciso, and F. J. Bermejo, J. Chem. Phys. **96**, 4625 (1992).
[44] H. J. C. Berendsen, J. P. M. Postma, W. F. Van Gunsteren, A. Di Nola, and J. R. Haak, J. Chem. Phys. **81**, 3684 (1984).
[45] M. P. Allen and D. J. Tildesley, *Computer Simulation of Liquids* (Clarendon Press, Oxford, 1987).
[46] R. Simha and R. F. Boyer, J. Chem. Phys. **37**, 1003 (1962).
[47] M. J. Mandell, J. P. McTague, and A. Rahman, J. Chem. Phys. **64**, 3699 (1976).

[48] W. Paul, D. Y. Yoon, and G. D. Smith, J. Chem. Phys. **103**, 1702 (1995).
[49] W. Brostow, J. P. Dussault, and B. L. Fox, J. Comput. Phys. **29**, 81 (1978).
[50] J. L. Finney, J. Comput. Phys. **32**, 137 (1979).
[51] M. Tanemura, T. Ogawa, and N. Ogita, J. Comput. Phys. **51**, 191 (1983).
[52] N. N. Medvedev, J. Comput. Phys. **67**, 223 (1986).